

1 **Quantitative reconstruction of summer precipitation using a Mid**
2 **Holocene $\delta^{13}\text{C}$ common millet record from Guanzhong Basin,**
3 **northern China**

4 Qing Yang^{1,2}, Xiaoqiang Li^{2*}, Xinying Zhou², Keliang Zhao² & Nan Sun³

- 5 1. School of Geography Science, Nanjing Normal University, Nanjing, 210023, China
6 2. Key Laboratory of Vertebrate Evolution and Human Origin of Chinese Academy of Sciences,
7 Institute of Vertebrate Paleontology and Paleoanthropology, Chinese Academy of Sciences,
8 Beijing, 100044, China
9 3. The School of Earth Science and Resources, Chang'an University, Xi'an, Sha'anxi, 710054,
10 China

11 *Correspondence and requests for materials should be addressed to X.L. (lixiaoqiang@ivpp.ac.cn)
12

13 **Abstract**

14 To quantitatively reconstruct Holocene precipitation for particular geographical
15 areas, suitable proxies and faithful dating controls are required. The fossilized seeds
16 of common millet (*Panicum miliaceum*) are found throughout the sedimentary strata
17 of northern China, and are suited to the production of quantitative Holocene
18 precipitation reconstructions: their isotopic carbon composition ($\delta^{13}\text{C}$) gives a
19 measure of the precipitation required during the growing season of summer (here the
20 interval from mid-June to September), and allows these seeds to be dated. We
21 therefore used a regression function, as part of a systematic study of the $\delta^{13}\text{C}$ of
22 common millet, to produce a quantitative reconstruction of Mid Holocene summer
23 precipitation in the Guanzhong Basin (107°40'~107°49'N, 33°39'~34°45'N). Our
24 results showed that mean summer precipitation at 7.7-3.4 ka BP was 353 mm, ~50
25 mm or 17% higher than present levels and the variability becomes increasing,
26 especially after 5.2 ka BP. Maximum mean summer precipitation peaked at 414 mm
27 during the period 6.1-5.5 ka BP, ~109 mm (or 36%) higher than today, indicating that
28 the EASM peaked at this time. This work can provide a new proxy for further
29 research into continuous paleoprecipitation sequences and the variability of summer
30 precipitation, which will promote the further research into the relation between early
31 human activity and environmental change.

32 **Keywords:** summer precipitation; quantitative reconstruction; Holocene; Chinese
33 Loess Plateau; common millet; stable carbon isotope
34

35 **Sect.**

36 **1 Introduction**

37 The reconstruction of global climate changes through history is an important part
38 of the Past Global Changes (PAGES) project. The Holocene, as the most recent
39 geological period, has the closest relation to human survival and development.
40 Quantitatively reconstructing climatic factors such as temperature and precipitation
41 provides an understanding of agricultural development and the human impact upon

42 the landscape and environment. However, instrumental records are insufficient for the
43 documenting of the drivers of climate change, since they cover only the past century
44 or so (DeMenocal, 2001). The quantitative reconstruction of temperature and
45 precipitation using climatic proxy records has therefore become the principal thrust of
46 PAGES research. To date, most continental paleoclimate studies have focused on
47 temperature (Porter and An, 1995; Guo *et al.*, 1996; Genty *et al.*, 2003; Wang *et al.*,
48 2008; Sun *et al.*, 2012). However, the increase in global surface temperatures has
49 tended to cause changes in precipitation and atmospheric moisture through changes in
50 atmospheric circulation, a more active hydrological cycle and an increasing water
51 holding capacity throughout the atmosphere (Dore, 2005). The availability of water,
52 one of the major challenges for the future, cannot be ignored, due to its significant
53 role in the hydrological cycle (Hatté and Guiot, 2005). To this end, we chose an area
54 key to the warm period of the Holocene to produce a quantitative precipitation
55 reconstruction for that geological time.

56 The Chinese Loess Plateau (CLP), located in a transition zone between a semi-
57 arid and semi-humid climate, is highly sensitive to changes in precipitation and has
58 thus long been a key area for precipitation reconstruction research. The precipitation
59 of the CLP, is, and has been, deeply impacted by the EASM. The EASM, an
60 important component of the Asian Summer Monsoon (ASM), plays an indispensable
61 role in the hydrological cycle over southern China. Various proxies have been adopted
62 in studies of the EASM during the Holocene. Due to their reliable chronology and
63 relatively easy dating, oxygen isotopes ($\delta^{18}\text{O}$) in speleothems from Chinese caves
64 have been taken as a robust measure of summer monsoon precipitation values (Wang
65 *et al.*, 2005a; Cheng *et al.*, 2009). However, the interpretation of these changes in the
66 $\delta^{18}\text{O}$ values of precipitation remains highly controversial; some scientists have
67 contended that the stalagmite $\delta^{18}\text{O}$ record from the EASM region may not record
68 EASM variability (Le Grande and Schmidt, 2009; Maher and Thompson, 2012; Tan,
69 2012; Caley *et al.*, 2014; Liu *et al.*, 2015). Fortunately, the precipitation in the CLP
70 can effectively reflect the intensity of the EASM variability due to its special location
71 (Liu *et al.*, 2015).

72 The quantitative precipitation reconstruction results obtained have been based
73 exclusively on climatic proxies derived from geological and biological records in the
74 CLP. In the western CLP, fossil charcoal records in the Tianshui Basin have
75 demonstrated that the mean annual precipitation (MAP) was 688-778 mm at 5.2-4.3
76 ka BP (Sun and Li, 2012). In the CLP's hinterland, magnetic susceptibility records
77 from the Luochuan profile have provided estimates of Holocene MAP varying
78 between 600 and 750 mm, with a mean value of 701 ± 74 mm (Lu *et al.*, 1994). In the
79 southern CLP, Guanzhong Basin MAP, as revealed by plant phytolith assemblies, was
80 700-800 mm during the Holocene, indicating a much more humid climate than
81 today's (Lu *et al.*, 1996). Further evidence from the transfer functions of geological
82 records and the intensity of pedogenesis has shown that Guanzhong Basin MAP
83 was >700 mm during the Holocene Optimum (Sun *et al.*, 1999; Zhao, 2003),
84 supporting the aforementioned results. However, due to their intrinsic limitations,
85 such as discontinuity or an indefinite response mechanism between the proxies and

86 climate change, these tentative proxies have not been extensively applied. Selecting
87 an effective proxy which evinces a reliable dating and a clear implication is crucial for
88 the quantitative reconstruction of paleoprecipitation. High-resolution pollen-based
89 quantitative precipitation results indicating EASM evolution have recently been
90 obtained from an alpine lake in northern China (Chen *et al.*, 2015). However, because
91 these are attributable solely to this unique environment, a regional quantitative
92 precipitation reconstruction, and therefore a new proxy, is still required.

93 Common millet (*Panicum miliaceum*), as the most representative agricultural
94 rain-fed crop of northern China, contains $\delta^{13}\text{C}$; this is sensitive to precipitation and
95 can thus effectively record precipitation during the growing season (Yang and Li,
96 2015). Rain-fed agriculture originated in the CLP, giving rise to the first
97 recognizably Chinese civilization. Many archeological relics from an unbroken
98 historical continuum are therefore found throughout the region (An, 1988).
99 Quantities of the fossilized seeds of common millet are well-preserved in the cultural
100 layers of these archeological sites (Zhao and Xu, 2004; Liu *et al.*, 2008; Lu *et al.*,
101 2009). Their stable $\delta^{13}\text{C}$ compositions, which remain little change because of the low
102 temperatures associated with carbonization, contain valuable information about
103 paleoclimate change and early agricultural activities (Yang *et al.*, 2011a, 2011b).
104 Common millet remains are therefore preferable for quantitatively reconstructing
105 Holocene precipitation in the CLP.

106 The Guanzhong Basin (Figure 1), in the southern CLP, was the cradle of
107 Neolithic culture and China's ancient civilization, and fostered the Laoguantai (~7.8-
108 6.9 ka BP), Yangshao (~6.9-5.0 ka BP) and Longshan (~5.0-4.0 ka BP) cultures (Ren
109 and Wu, 2010), the pre-Zhou culture (~3.5-3.0 ka BP) (Lei, 2010), and the Zhou
110 dynasties. Due to the intensity of early agricultural activity, huge quantities of
111 common millet remains have been preserved in numerous, continuously-occupied
112 cultural sites. Charred common millet seeds are the most abundant resource found in
113 the samples collected in this study from these cultural layers.

114 In this study, common millet remains, from five sections characterized by
115 continuous and well-developed sedimentation at typical archeological sites, including
116 the Baijia, Huiduipo, Manan, Beiniu and Nansha sites (Figure 1), were sampled as
117 part of a systematic study of $\delta^{13}\text{C}$ records; quantitative precipitation reconstructions
118 for the Holocene were then based upon a transfer function between the $\delta^{13}\text{C}$ of
119 modern common millet and precipitation, providing a scientific basis for predicting
120 future climate change and its possible impact.

122 **2 The rationale behind using common millet $\delta^{13}\text{C}$ for precipitation** 123 **reconstruction**

124 The $\delta^{13}\text{C}$ values of common millet seeds reflect the ^{13}C of photosynthetic
125 materials during not only their formative and mature stages, but also their vegetative
126 stage. The growing season of modern common millet in the Guanzhong Basin lasts
127 from June to September. The seed kernel's formative and mature stages occur soon
128 after pollination of the blossom. With an increase in kernel size, photosynthetic
129 material as well as pre-accumulated organic material is transferred to kernels from

130 stems, leaves and spikes (Chai, 1999). Therefore, millet $\delta^{13}\text{C}$ reflects the
131 environmental conditions extant during the growing season from mid-June to the end
132 of September, or 110 days in total.

133 Carbon isotope composition of fossilized plant remains is a useful proxy for the
134 reconstruction of local paleoclimatic changes, especially when using $\delta^{13}\text{C}$ values from
135 plants which experience a single mode of photosynthesis. Common millet grains have
136 been widely and continuously preserved throughout the Holocene in northern China.
137 Fossilized millet seeds were generally formed by baking at low temperatures ($\sim 250^\circ\text{C}$)
138 (Yang *et al.*, 2011a), and deposited in strata over long time periods with limited
139 interaction with the buried environment. The observed $\delta^{13}\text{C}$ values of charred
140 common millet formed at $\sim 250^\circ\text{C}$ were 0.2‰ lower than those of the source samples,
141 and much less than the natural variation typically found in wood (Yang *et al.*, 2011b).
142 The $\delta^{13}\text{C}$ signatures conserved in charred common millet are thus reflective of the true
143 environment.

144 The carbon isotope composition of plants ($\delta^{13}\text{C}_p$) is affected by both
145 physiological characteristics and environmental factors. The $\delta^{13}\text{C}$ of C_3 plants
146 responds to environmental factors, such as atmospheric CO_2 pressure, O_2 partial
147 pressure, temperature, light and precipitation, by dominating the ratio of the
148 intercellular and ambient partial pressure of CO_2 (c_i/c_a) with the opening and closing
149 of leaf stomata (Körner and Diemer, 1987; Körner and Larcher, 1988; Körner *et al.*,
150 1989; Farquhar *et al.*, 1989; Dawson *et al.*, 2002). However, the $\delta^{13}\text{C}$ of C_4 plants
151 depends not only on c_i/c_a but also on how much CO_2 and HCO_3^- in bundle sheath cells
152 leaks into the mesophyll cells (called leakiness ϕ), which is determined by its
153 physiological characteristics (Hubick *et al.*, 1990). When ϕ is larger/smaller than 0.37,
154 there is a positive/negative correlation between $\delta^{13}\text{C}_p$ and c_i/c_a (Ubierna *et al.*, 2011).
155 Under water stress, the ϕ of the common millet, belonging to the NADP-ME
156 subgroup of C_4 plants, is likely larger than 0.37 (Schulze *et al.*, 1996; Yang and Li,
157 2015). This may account for the significantly positive relation between the $\delta^{13}\text{C}$ of
158 common millet and precipitation (Yang and Li, 2015).

159 Limited precipitation and soil humidity are the most important environmental
160 factors affecting the growth of plants in arid and semi-arid areas (Hadley and Szarek,
161 1981; Ehleringer and Mooney, 1983; Murphy and Bowman, 2009). For C_4 species in
162 the arid regions of northwestern China, $\delta^{13}\text{C}_p$ tends to decrease with decreasing soil
163 water availability (Wang *et al.*, 2005b). For common millet, although altitude,
164 precipitation and water availability have a significant correlation with $\delta^{13}\text{C}$ according
165 to correlation analysis, precipitation was the critical control of $\delta^{13}\text{C}$, based on
166 functional mechanism analysis (Yang and Li, 2015). The plants' physiological
167 characteristics and morphological adaptability showed that the stomatal, and some
168 non-stomatal, factors of common millet are sensitive to water status, causing the $\delta^{13}\text{C}$
169 of the organic material to change with precipitation. This rationale establishes an
170 important theoretical foundation whereby the $\delta^{13}\text{C}$ of common millet can serve as an
171 effective indicator of paleoprecipitation.

172

173 3 Methods

174 **Sampling.** All the ancient common millet remains used in this study were found
175 at five archeological sites in the Guanzhong Basin, *i.e.* the Baijia, Huiduipo, Manan
176 Beiniu and Nansha sites (State Cultural Relics Bureau, 1998).

177 The Guanzhong Basin is located southern of the CLP and is bordered on the
178 south by the Qinling Mountains and the north by the Beishan Mountain and spanned
179 30-80 km; from Baoji Valley at the west end to Tongguan at the east end, spanning
180 360 km. The topography is flat and the landscape consists mostly of river terraces and
181 loess table land at an altitude of 326-600 m. The present-day Guanzhong Basin is
182 characterized by semi-humid and semi-arid climatic conditions strongly influenced by
183 the monsoon. Summer monsoon rainfall accounts for most of the annual precipitation
184 and falls primarily in June-August; the climate is therefore characterized by cold, dry
185 winters and moist, warm summers. Mean annual temperature (MAT) in the
186 Guanzhong area is ca. 13°C, MAP is ~575 mm and mean annual relative humidity
187 (MARH) is 70%. Precipitation data from the Guanzhong Basin for the period 1951-
188 2011 were analyzed (Figure 2). The results showed that the precipitation for mid-June
189 to September was between 110-526 mm, with a mean of 305 mm. The 95%
190 confidence interval for this mean is between 279-332 mm, ruling out the extreme
191 values of abnormal years.

192 The Baijia site, located on the secondary river terrace of the northern bank of
193 River Wei, contains early Laoguantai cultural remains. The area is ca. 120,000 m² and
194 the thickness of the cultural layer is between 0.4 m and 1.2 m. The Huiduipo site
195 includes Banpo-type remains from the Yangshao culture. The area is ca. 60,000 m²,
196 the thickness of the cultural layer is ca. 2 m, and there is partial exposure of ash pits,
197 residential areas and graves. The Manan site, located on tableland at the intersection
198 of the Jinghe and Weihe rivers, exhibits Yangshao cultural remains. MN is ca. 16,000
199 m² in area, and the thickness of the cultural layer is between 2 m and 5 m, with a
200 dense distribution of ash pits. The Beiniu site partly contains Longshan cultural
201 remains. Its area is 200,000 m², and the thickness of its cultural layer is ca. 1m. The
202 Nansha site is mainly characterized by Shang Dynasty remains. It is ca. 300,000 m² in
203 area and the thickness of its cultural layer is between 1.9 m and 2.7 m (State Cultural
204 Relics Bureau, 1998). All sampling sections are described in Figure 1.

205 Five sections characterized by continuous and well-developed sedimentation
206 were selected for sampling at the Baijia, Beiniu, Huiduipo, Manan and Nansha sites.
207 The slice sampling were applied to continuously sampling and the interval was 10 cm
208 for the Baijia and Nansha sections, and 20 cm for the Beiniu, Huiduipo and Manan
209 sections (Figure 1). Forty litre sample bags were filled with sufficient quantities of
210 sedimentary material to screen through a 50-mesh sieve to obtain samples using
211 flotation (Tsuyuzaki, 1994). Different archeological remains were separated in the
212 laboratory after air-drying. Agricultural seeds were identified and picked out under the
213 stereomicroscope, then marked in order according to sampling depth. The number of
214 remnant common millet samples derived from all five sections are listed in Table 1.

215 **Stable $\delta^{13}\text{C}$ analysis.** Stable $\delta^{13}\text{C}$ composition analyses were carried out on all 67
216 serial and bulk common millet samples from the five sections, each composed of three
217 to five grains, without lemma. Each sample portion was placed in a beaker and
218 covered with a 1% hydrochloric acid solution to remove any carbonates. The samples
219 were then washed with deionized water to $\text{pH} > 5$ and oven dried at 40°C for 24 h. The
220 dried samples were ground in an agate mortar and homogenized, then vacuum-sealed
221 in a quartz tube with copper oxide and silver foil and combusted for at least 4 h at
222 850°C . The CO_2 gas from the combustion tube was extracted and cryogenically
223 purified. The isotopic ratio of the extracted CO_2 gas was determined using a MAT-253
224 gas source mass spectrometer with a dual inlet system at the Institute of Earth
225 Environment, Chinese Academy of Sciences.

226 All isotope ratios were expressed using the following δ notation:

$$227 \quad \delta^{13}\text{C}(\text{‰}) = [(\text{R}_{\text{sample}} - \text{R}_{\text{std}}) / \text{R}_{\text{std}}] \times 1000 \quad \text{Eq. (1)}$$

228 The isotopic standard used was Vienna Pee Dee Belemnite (VPDB); analytical
229 precision at the 1σ level was reported as 0.2‰.

230 **Radiocarbon dating.** AMS ^{14}C dating was conducted on one charcoal fragment
231 and one charred seed of common millet from the Baijia section, five charred seeds
232 each from the Huiduipo and Beiniu sections, one charred seed from the Manan
233 section, and three charred seeds from the Nansha section.

234 The charcoal and seed samples were pretreated by washing in 10% NaOH and
235 10% HCl and reduced to neutral pH. They were then converted to graphite and
236 radiocarbon ages were calculated after measurement in the STAR Accelerator at the
237 Australian Nuclear Science and Technology Organisation (ANSTO). AMS ^{14}C dates
238 were calibrated using Calib Rev 7.0.4 software and the INTCAL13 dataset (Reimer *et*
239 *al.*, 2013).

240 **Processing data of age model.** On the basis that the depth-based linear
241 interpolation method was not fit for the dating of cultural layers because of potential
242 disturbance, all common millet remnant samples were divided into several groups to
243 guarantee at least one dating dataset for each group (Figure 3a), as follows: samples
244 from adjacent depths with close $\delta^{13}\text{C}$ values were placed in the same group, allowing
245 a greater difference between each group (One-factor Analysis of Variance (one-way
246 ANOVA), $P < 0.05$).

247 **Quantitative modeling method and data analysis.** The results for $\delta^{13}\text{C}$ values
248 in the seeds of modern millet grown on the CLP (Yang and Li, 2015) demonstrated
249 that the $\delta^{13}\text{C}$ of common millet has a significant positive correlation with
250 precipitation. In this study, standard major axis regression analysis (SMA) was
251 applied to establish a regression model between the $\delta^{13}\text{C}$ of modern common millet
252 and precipitation during growing seasons. Statistical analyses were conducted using
253 SMATR software (Version 2.0) (Falster *et al.*, 2006). Other statistical analyses used
254 SPSS 15.0 for Windows and OriginPro 8.0 software. Unless otherwise stated,
255 differences were considered statistically significant when $P < 0.05$.

256

257 **4 Results**

258 The radiocarbon results (Table 2) show that the ages of the sampled cultural

259 layers were usually correspondent with archeological periodization. Common millet
260 remains sampled from cultural layers of Guanzhong Basin in our study have $\delta^{13}\text{C}$
261 values ranging from -11.1‰ to -9.3‰ (Figure 3a), with a mean of $-10.2\pm 0.4\%$ ($n=$
262 66, $SD=\pm 1\sigma$), without considering the anomaly value of -8.8‰ analyzed by Boxplot
263 using SPSS statistical software (Figure 3b), which may be affected by the local
264 environment. The $\delta^{13}\text{C}$ composition of modern common millet from the central and
265 western CLP measured in 2008 ranged from -13.9‰ to -12.5‰, with a mean of -
266 $13.2\pm 0.5\%$ ($n=15$, $SD=\pm 1\sigma$) (Yang and Li, 2015). It can thus be seen that the $\delta^{13}\text{C}$
267 values of common millet remains are more positive than those of modern millet by \sim
268 2.9‰.

269 The ^{13}C composition of plants results from a combination of carbon isotope
270 fractionation and source carbon isotope composition. Therefore, $\delta^{13}\text{C}$ changes in the
271 atmosphere, as a part of total CO_2 , are an important factor impacting upon the $\delta^{13}\text{C}$
272 values in plants (O'Leary, 1988; Farquhar, 1989; Araus and Buxo, 1993). Considering
273 our atmosphere is a perfect blender, we adopted the global mean $\delta^{13}\text{C}$ value of
274 atmospheric CO_2 , -8.2‰, in 2011 (Cuntz, 2011), which was three years after
275 sampling. The $\delta^{13}\text{C}$ values of atmospheric CO_2 in the Holocene, from 11 ka BP to the
276 pre-industrial age, show only a slight change, usually ranging between -6.1‰ and -
277 6.6‰, with a mean value of $-6.4\pm 0.15\%$ (Marino *et al.*, 1992; Leuenberger *et al.*,
278 1992). $\sim 1.8\%$ higher than present-day atmospheric CO_2 $\delta^{13}\text{C}$ values of -8.2‰
279 (Farquhar *et al.*, 1989; Keeling and Whorf, 1992). After correcting for the change in
280 atmospheric CO_2 $\delta^{13}\text{C}$ (1.8‰), the millet $\delta^{13}\text{C}$ values for Holocene millet from the
281 Guanzhong Basin are equivalent to modern caryopsis values of $-12.0\pm 0.4\%$, and are
282 therefore $\sim 1.2\%$ less depleted in $\delta^{13}\text{C}$ than modern caryopsis (for the t test, $t=21.39$).

283 The regression function between $\delta^{13}\text{C}$ and precipitation for the common millet
284 growing season was established using SMA as follows (Figure 4):

$$285 \quad \delta^{13}\text{C} (\text{‰}) = 0.0077P_{\text{gs}} - 14.76, \quad r^2 = 0.56, \quad P < 0.001 \quad \text{Eq.(2)}$$

286 Where P_{gs} denotes the precipitation of millet growth seasons. The function's
287 gradient indicated that the precipitation coefficient was 0.77‰/100 mm, implying
288 that, within physiological adaptation parameters, there would be a $\sim 0.77\%$ increase in
289 $\delta^{13}\text{C}$ with a 100 mm increase in precipitation. The $\delta^{13}\text{C}$ values yielded by ancient
290 common millets are higher than those of modern common millet seeds, suggesting
291 that these ancient plants grew in a more humid environment than today's.

292 Common millet remains from archeological sites were divided into a total of 11
293 groups (Table 3). Mean $\delta^{13}\text{C}$ values for common millet remains were calculated for
294 each group. Results showed that the minimum value was $-10.6\pm 0.2\%$, and the
295 maximum value $-9.6\pm 0.1\%$, for common millet growing between 7.7 ka BP and 3.4
296 ka BP. After correcting for the change in the atmospheric CO_2 $\delta^{13}\text{C}$ (1.8‰), the range
297 of mean $\delta^{13}\text{C}$ values for ancient millet *vis-à-vis* modern plants was between -
298 $12.4\pm 0.2\%$ and $-11.4\pm 0.1\%$. By applying the regression model based on the $\delta^{13}\text{C}$ and
299 precipitation values for modern common millet during its growing season, we were
300 able to extract paleoprecipitation values for the growing seasons of ancient crops for
301 certain time periods.

302 These paleoprecipitation values were reconstructed by applying the corrected

303 $\delta^{13}\text{C}$ values for the ancient millet to the regression equation (Eq. 2) which expresses
304 the relation between the $\delta^{13}\text{C}$ of common millet and precipitation. The results showed
305 that the precipitation for the growing seasons of ancient millet during the period 7.7-
306 3.4 ka BP varied from 240 mm to 477 mm, with a mean of 354 mm (Table 3).

307

308 **5 Discussion**

309 Ancient equivalent-seed $\delta^{13}\text{C}$ values, ranging from $-12.4\pm 0.2\%$ to $-11.4\pm 0.1\%$,
310 are $\sim 1\text{--}2\%$ higher than those for modern millet in the area. Paleoprecipitation
311 reconstructed from the regression function shows that precipitation of millet growth
312 seasons at 7.7-3.4 ka BP was between 242 and 475 mm, with a mean of 353 mm.
313 Summer paleoprecipitation values show that the climate was much more humid than it
314 is today, which was 305 mm on average during 1951-2011, with mean precipitation
315 ~ 50 mm, or 17%, higher. A peak mean summer precipitation of 442 mm was reached
316 at ~ 5.7 ka BP; even the lowest value of 311 mm ~ 6.5 ka BP was higher than today's
317 mean value. Summer precipitation during the Mid Holocene (7.7-3.4 ka BP) in the
318 Guanzhong Basin exhibited a systemic increase.

319 The reconstructed summer precipitation also fluctuates significantly and
320 becomes more and more variable, especially after 5.2 ka BP. However, there were
321 three markedly humid periods, i.e. 6.1-5.5 ka BP, ~ 4.2 ka BP, and ~ 3.6 ka BP (Figure
322 5). The period 6.1-5.5 ka BP had the most abundant summer precipitation, which was
323 414 mm, i.e. 109 mm, or 36%, higher than today. At ~ 4.1 ka BP, the precipitation was
324 397 ± 11 mm, 92 mm or 30% higher than at present; at ~ 3.6 ka BP, the precipitation
325 was 414 ± 45 mm, 36% higher than at present.

326 The period 6.1-5.5 ka BP, being the most markedly humid period, probably
327 marks the Holocene Climate Optimum in the Guanzhong Basin; this was also when
328 the Yangshao Culture flourished, with archeological finds indicating that there were as
329 many villages in the area as there are today. It is worth noting that the anomalous high
330 value at ~ 4.1 ka BP and ~ 3.6 ka BP, may indicate rapidly-developing climatic events,
331 correspondent with other global records (Cullen and DeMenocal, 2000; Mayewski et
332 al., 2004; Wu and Liu, 2004).

333 The instrumental data for the last 61 years (1951-2011) indicate that precipitation
334 in the Guanzhong Basin occurs mainly in the summer (Figure 2). The current inland
335 flow of warm/humid air dominated by the EASM during the summer (June through
336 September) delivers $\sim 58\%$ of the total annual precipitation. The area is a typical
337 monsoon precipitation area, and summer precipitation here is therefore sensitive to
338 variations in the EASM.

339 Previous studies of various climatic proxies including stalagmite $\delta^{18}\text{O}$, lacustrine
340 sediments and loess-paleosols all indicate that the CLP had plenty of rain in the
341 Holocene and was much more humid during the Mid Holocene (Shen *et al.*, 2005;
342 Wang *et al.*, 2005a; Wang *et al.*, 2008; Wang *et al.*, 2014; Chen *et al.*, 2015). The
343 frequency of paleosol development increased during $\sim 8.6\text{--}3.2$ ka in the CLP (Wang *et al.*,
344 2014). The eolian-sand activities in the sandlands located to the north of the CLP
345 decreased from $\sim 8.6\text{--}3.2$ ka BP (Wang *et al.*, 2014; Yang *et al.*, 2012), whilst the
346 vegetation coverage of the desert/loess transitional zone increased in this interval

347 (Yang *et al.*, 2015). These various proxy records infer that the EASM was stronger
348 during the Mid Holocene, but the amplitude of any variations in the EASM remains
349 difficult to assess.

350 Our quantitative reconstructions of summer precipitation based on millet $\delta^{13}\text{C}$
351 indicate that EASM intensity peaked during 6.1-5.5 ka BP. The strongest summer
352 monsoon brought the wettest millet growth seasons, with 36% higher precipitation
353 than today's. More evidence supporting our contention comes from the tree pollen
354 records from lake sediments around the CLP, which respond more directly to changes
355 in the EASM than the other records because trees on the margins of monsoonal
356 regions are sensitive to variations in monsoonal precipitation. Pollen records from
357 Qinghai Lake, located to the west of the Guanzhong Basin and on the modern
358 monsoon margins, indicate a wet interval during 7.4-4.5 ka BP, culminating in a peak
359 at 6.5 ka BP (Figure 6a) (Shen *et al.*, 2005). Although the increase in precipitation
360 cannot be assessed, the general trend is comparable with our $\delta^{13}\text{C}$ -based precipitation
361 reconstruction results. The percentage of broadleaf trees from pollen record in the
362 Gonghai Lake (on the northeastern margins of the CLP; Figure 6b), indicate that the
363 peak monsoonal period occurred during ~7.8-5.3 ka BP, with an average annual
364 precipitation of 574 mm (Figure 6c), ~30% higher than the modern value (Chen *et al.*,
365 2015). The increase in precipitation is highly consistent with our reconstruction
366 results. More evidence from PMIP2 (the second phase of the Paleoclimate Modeling
367 Intercomparison Project) coupled with Mid Holocene simulations showed that the
368 summer precipitation associated with the EASM increased throughout most of China
369 ~6 ka BP and the greatest increases in precipitation seen in the region, *i.e.* the
370 southern margins of the Tibetan Plateau, and southeastern coastal area of China,
371 which experienced precipitation increases of >1.5 mm/day and 0.7 mm/day (or 547.5
372 mm/yr and 255.5 mm/yr), respectively (Zhang and Liu, 2009). According to the
373 result, it can be inferred the increase in precipitation in the Guanzhong Basin was
374 lower than 255.5 mm/yr at that time. These multiple lines of evidence corroborate our
375 reconstructions, not only *vis-à-vis* changes in precipitation during the Holocene, but
376 also their quantitative accuracy.

377

378 **5 Conclusions**

379 $\delta^{13}\text{C}$ of common millet from archaeological layer can effectively record
380 precipitation during millet growing season. Summer precipitation at 7.7-3.4 ka BP
381 reconstructed using the $\delta^{13}\text{C}$ values of common millet was 353 mm, ~50 mm, or
382 17%, higher than at present. Maximum mean summer precipitation peaked at 414 mm
383 during the period 6.1-5.5 ka BP, ~109 mm (or 36%) higher than today, indicating that
384 the EASM peaked at this time. Furthermore, the increasing variability of summer
385 precipitation was visible, especially after 5.2 ka BP. The work provides a new proxy
386 for establishing the paleoprecipitation record.

387 Charred common millet remains continuously exist in the archaeological layers
388 since around 10 ka in northern China. Not only the common millet can provide a
389 reliable dating framework, but also the continuous $\delta^{13}\text{C}$ -based paleoprecipitation
390 sequences could be quantitatively reconstructed. This, in turn, can allow regional

391 comparisons, providing a scientific foundation for promoting further research and
392 helping to understand the processes and mechanisms of the EASM, as well as the
393 relation between early human activity and environmental change.

394

395 **Authorial contributions**

396 X. Q. L.: overall coordination of writing, sampling, ¹⁴C dating and paleoprecipitation
397 reconstruction; Q. Y.: writing, sampling, data processing and paleoprecipitation
398 reconstruction; X. Y. Z. and K. L. Z.: sampling and data processing; N. S.: sampling and ¹⁴C
399 dating. All authors reviewed the manuscript.

400

401 **Acknowledgements**

402 This study was supported by the National Basic Research Program of China (Grant No.
403 2015CB953804, 2015CB953803), the National Natural Science Foundation of China (Grant
404 Nos. 41301042, 41372175) and the National Science Fund for Talent Training in Basic
405 Science (Grant No. J1210008). We thank Prof. John Dodson for AMS¹⁴C dating support, and
406 Dr. Ying Xi for assistance with collecting the original meteorological data.

407

408 **References**

- 409 An, Z. M.: Prehistoric agriculture in China, *Acta. Archaeol. Sin.*, 4, 369–381, in Chinese, 1988.
410 Arais, J. L., and Buxo, R. Changes in carbon isotope discrimination in grain cereals from the
411 north-western Mediterranean Basin during the past seven millennia, *Aust. J. Plant. Physiol.*, 20,
412 117-128, 1993.
413 Caley, T., Roche, D. M. and Renssen, H.: Orbital Asian summer monsoon dynamics revealed
414 using an isotope-enabled global climate model, *Nat. Commun.*, 5, 5371, 2014.
415 Chai, Y.: Broomcorn millet, Chinese Agriculture Press, Beijing, China, 47-70, 1999.
416 Chen, F. H., Xu, Q. H., Chen, J.H., Birks, H. J. B., Liu, J. B., Zhang, S. R., Jin, L., An, C. B.,
417 Telford, R. J., Cao, X. Y., Wang Z. L., Zhang, X. J., Selvaraj, K., Lu, H. Y., Li, Y.C., Zheng, Z.,
418 Wang, H. P, Zhou, A.F., Dong, G.H., Zhang, J. W., Huang, X. Z., Bloemendal, J., and Rao,
419 Z.G.: East Asian summer monsoon precipitation variability since the last deglaciation, *Sci. Rep.*,
420 5, 11186, 2015.
421 Cheng, H., Edwards, R.L., Broecker, W. S., Denton, G.H., Kong, X., Wang, Y., Zhang, R., Wang,
422 X.: Ice Age Terminations, *Science*, 326, 248-252, 2009.
423 Cullen, H. M, deMenocal, P. B.: North Atlantic influence on Tigris-Euphrates stream flow,
424 *International Journal of Climatology*, 20, 853-863, 2000.
425 Cuntz, M.: Carbon cycle: A dent in carbon's gold standard, *Nature*, 477, 547–548, 2011.
426 Dawson, T.E., Mambelli, S., Plamboeck, A. H., Templer, P. H., and Tu, K. P.: Stable Isotopes in
427 *Plant Ecology*, *Annu. Rev. Ecol. Syst.*, 33, 507–559, 2002.
428 DeMenocal, P. B.: Cultural responses to climate change during the late Holocene, *Science*, 292,
429 667-673, 2001.
430 Dore, M. H. I.: Climate change and changes in global precipitation patterns: What do we know?,
431 *Environ. Int.*, 31, 1167-1181, 2005.
432 Ehleringer, J. R., and Mooney, H. A.: Photosynthesis and productivity of desert and Mediterranean
433 climate plants, *Encyclopedia Plant Physiol (NS)*, Springer-Verlag, New York, 205-231, 1983.

434 Falster, D. S., Warton, D. I., and Wright, I. J.: User's guide to SMATR: Standardised Major Axis
435 Tests & Routines Version 2.0, Copyright 2006, 2006,
436 <http://www.bio.mq.edu.au/ecology/SMATR/>

437 Farquhar, G. D., Ehleringer, J. R., and Hubick, K. T.: Carbon isotope discrimination and
438 photosynthesis, *Annu. Rev. Plant Physiol. Mol. Biol.*, 40, 503-537, 1989.

439 Genty, D., Blamart, D., Ouahdi, R., Gilmour, M., Baker, A., Jouzel, J., Van-Exter, S.: Precise
440 dating of Dansgaard–Oeschger climate oscillations in western Europe from stalagmite data,
441 *Nature*, 421, 833-837, 2003.

442 Guo, Z. T., Liu, T., Guiot, J., Wu, N., L. H., Han, J., Liu, J., Gu, Z.: High frequency pulses of East
443 Asian monsoon climate in the last two glaciations: link with the North Atlantic, *Clim. Dynam.*,
444 12, 701-709, 1996.

445 Hadley, N.F., and Szarek, S.R.: Productivity of desert ecosystems, *BioScience*, 31, 747-753, 1981.

446 Hatté, C., and Guiot, J.: Palaeoprecipitation reconstruction by inverse modelling using the isotopic
447 signal of loess organic matter: application to the Nußloch loess sequence (Rhine Valley,
448 Germany), *Clim Dynam*, 25, 315-327, 2005.

449 Hubick, K.T., Hammer, G. L., Farquhar, G. D., Wade, L. J., von Caemmerer, S., and Henderson, S.
450 A.: Carbon isotope discrimination varies genetically in C4 species, *Plant. Physiol.*, 92, 534–537,
451 1990.

452 IPCC: Climate Change 2007: The Physical Science Basis, Solomon, S. et al. Cambridge, 2007

453 Keeling, C. D., and Whorf, T. P. in: Atmospheric CO₂ – modern record, Mauna Loa, edited by:
454 Boden, T A, Sepanski, R. J. and Stoss, F. W.: Trends 91: A Compendium of Data on Global
455 Change, ORNL/CDIAC-46, Carbon Dioxide Information Analysis Center, Oak Ridge National
456 Laboratory, Oak Ridge, Tennessee, USA, 12-15, 1992.

457 Körner, C. H., and Diemer, M.: *In situ* photosynthetic responses to light, temperature and carbon
458 dioxide in herbaceous plants from low and high altitude, *Funct. Ecol.*, 1(3), 179-194, 1987.

459 Körner, C. H., and Larcher, W. Plant life in cold climates, *Symp Soc Exper Biol.*, 42, 25–57,
460 1988.

461 Körner, C. H., Newmayer, M., Palaez Menendez-Reidl, S., and Smeets-Scheel, A.: Functional
462 morphology of mountain plants, *Flora*, 182, 353-383, 1989.

463 LeGrande, A., and Schmidt, G.: Sources of Holocene variability of oxygen isotopes in
464 paleoclimate archives, *Clim. Past*, 5, 441-455, 2009.

465 Lei, X. S.: Pre-Zhou culture exploration, Science Press, Beijing, China, in Chinese, 2010.

466 Leuenberger, M., Siegenthaler, U., and Langway, C. C.: Carbon isotope composition of
467 atmospheric CO₂ during the last ice age from an Antarctic ice core, *Nature*, 357, 488-490, 1992.

468 Liu, C. J., Jin, G. Y., and Kong, Z. C.: Archaeobotany — Research on Seeds and Fruits, Science
469 Press, Beijing, China, pp. 160-171, 2008.

470 Liu, J.B., Chen, J.H., Zhang, X. J., Li, Y., Rao, Z. G., and Chen, F. H.: Holocene East Asian
471 summer monsoon records in northern China and their inconsistency with Chinese stalagmite
472 $\delta^{18}\text{O}$ records, *Earth-Sci. Rev.*, 148, 194-208, 2015.

473 Lu, H. Y., Han, J. M., Wu, N. Q., and Guo Z. T.: The analysis of modern soil magnetic
474 susceptibility and its paleoclimate significance, *Sci. China, Ser. B*, 24(12), 1290-1297, in
475 Chinese, 1994.

476 Lu, H. Y., Wu, N. Q., Liu, T. S., Han, J. M., and Qin X. G.: Seasonal climatic variation recorded
477 by phytolith assemblages from the Baoji loess sequence in central China over the last 150 000,

478 Sci. China, Ser. D, 39(6), 629-639, 1996.

479 Lu, H. Y., Zhang, J. P., Liu, K.-B., Wu, N. Q., Li, Y. M., Zhou, K. S., Ye, M. L., Zhang, T. Y.,
480 Zhang, H. J., Yang, X. Y., Shen, L. C., Xu, D. K., Li, Q., and Piperno, D. R.: Earliest
481 domestication of common millet (*Panicum miliaceum*) in East Asia extended to 10,000 years
482 ago, P. Natl. Acad. Sci. U.S.A., 18, 7367-7372, 2009.

483 Maher, B. A., and Thompson, R.: Oxygen isotopes from Chinese caves: records not of monsoon
484 rainfall but of circulation regime, J. Quat. Sci., 27, 615-624, 2012.

485 Marino, B. D., McElroy, M. B., Salawitch, R. J., and Spaulding, W. G.: Glacial-to-interglacial
486 variations in the carbon isotopic composition of atmospheric CO₂, Nature, 357, 461-466, 1992.

487 Mayewski, P. A., Rohling, E. E., Stager, J. C., Karlén, W., Maasch, K. A., Meeker, L. D.,
488 Meyerson, E. A., Gasse, F., van Kereveld, S., Holmgren, K., Lee-Thorp, J., Rosqvist, G., Rack,
489 F., Staubwasser, M., Schneider, R. R., and Steig, E. J.: Holocene climate variability, Quatern.
490 Res., 504 62(3), 243-255, 2004.

491 Murphy, B. P., and Bowman, D. M. J. S.: The carbon and nitrogen isotope composition of
492 Australian grasses in relation to climate, Funct Ecol, 23, 1040-1049, 2009.

493 O'Leary, M. H.: Carbon isotopes in photosynthesis, BioScience, 38, 323-336, 1988.

494 Porter, S. C., and An, Z. S.: Correlation between climate events in the North Atlantic and China
495 during the last glaciation, Nature, 375, 305-308, 1995.

496 Reimer, P. J., Bard, E., Bayliss, A., Beck, J. W., Blackwell, P. G., Ramsey, C. B., Buck, C. E., Hai
497 C., Edwards, R. L., Friedrich, M., Grootes, P. M., Guilderson, T. P., Hafliðason, H., Hajdas, I.,
498 Hatté, C., Heaton, T. J., Hoffmann, D. L., Hogg, A. G., Hughen, K. A., and Kaiser, K. F.:
499 IntCal13 and Marine13 radiocarbon age calibration curves 0-50,000 years cal BP, Radiocarbon
500 55(4), 1869-1887, 2013.

501 Ren, S. N., and Wu, Y. L.: The Neolithic Volume of Chinese Archaeology, Chinese Social Science
502 Press, Beijing, China, in Chinese, 2010.

503 Schulze, E.-D., Ellis, R., Schulze, W., Trimborn, P., and Ziegler, H.: Diversity, metabolic types
504 and $\delta^{13}\text{C}$ carbon isotope ratios in the grass flora of Namibia in relation to growth form,
505 precipitation and habitat conditions, Oecologia, 106, 352-369, 1996.

506 Shen, J., Liu, X. Q., Wang, S. M., and Ryo, M.: Palaeoclimatic changes in the Qinghai Lake area
507 during the last 18,000 years, Quat. Int., 136, 131-140, 2005.

508 State Cultural Relics Bureau (ed): Atlas of Chinese Cultural Relics: Shannxi Municipality, Xi'an
509 Map Press, Xi'an, China, in Chinese, 1998.

510 Sun, J. M., Diao, G. Y., Wen, Q. Z., and Zhou, H. Y.: A preliminary study on quantitative
511 estimate of Palaeoclimate by using geochemical transfer function in the Loess Plateau,
512 Geochim, 28(3), 265-272, in Chinese, 1999.

513 Sun, N., Li, X. Q., Dodson, J., Zhou, X. Y., Zhao, K. L., Yang, Q.: Plant diversity of the Tianshui
514 Basin in the western Loess Plateau during the mid-Holocene – charcoal records from
515 archaeological sites, Quatern. Int, 308-309, 27-35, 2012.

516 Sun, N., and Li, X. Q.: The quantitative reconstruction of the palaeoclimate between 5200 and
517 4300 cal yr BP in the Tianshui Basin, NW China, Clim. Past, 8, 625-636, 2012.

518 Tan, M.: Circulation effect: response of precipitation $\delta^{18}\text{O}$ to the ENSO cycle in monsoon
519 regions of China, Clim. Dyn., 42, 1067-1077, 2012.

520 Tsuyuzaki, S.: Rapid seed extraction from soils by a flotation method, Weed Res., 34, 433-436,
521 1994.

522 Ubierna, N., Sun, W., and Cousins, A. B.: The efficiency of C₄ photosynthesis under low light
523 conditions: assumptions and calculations with CO₂ isotope discrimination, *J. Exp. Bot.*, 1–16,
524 2011.

525 Wang, H., Chen, J., Zhang, X., and Chen, F.: Palaeosol development in the Chinese Loess Plateau
526 as an indicator of the strength of the East Asian summer monsoon: Evidence for a mid-
527 Holocene maximum, *Quaternary International*, 334, 155-164, 2014.

528 Wang, Y. J., Cheng H., Edwards, R. L., He Y. Q., Kong, X. G., An, Z. S., Wu, J. Y., Kelly, M. J.,
529 Dykoski, C. A., and Li, X. D.: The Holocene Asian monsoon: links to solar changes and North
530 Atlantic climate, *Science*, 308, 854-857, 2005a.

531 Wang, G.A., Han, J. M., Zhou, L. P., Xiong, X. G, and Wu, Z. H.: Carbon isotope ratios of plants
532 and occurrences of C₄ species under different soil moisture regimes in arid region of Northwest
533 China, *Physiol.Plant.*, 125, 74–81, 2005b.

534 Wang, Y. J., Cheng, H., Edwards, R. L., Kong, X. G., Shao, X. H., Chen, S. T., Wu, J. Y., Jiang,
535 X. Y., Wang, X. F., and An, Z. S.: Millennial- and orbital-scale changes in the East Asian
536 monsoon over the past 224,000 years, *Nature*, 451, 1090-1093, 2008.

537 Warton, D. I., Wright I. J., Falster, D. S., and Westoby, M.: Bivariate Line-fitting methods for
538 allometry, *Biol. Rev.*, 81, 259-291, 2006.

539 Wu, W. X., Liu, T. S.: Possible role of the “Holocene Event 3” on the collapse of Neolithic
540 Cultures around the Central Plain of China, *Quaternary International*, 117, 153-166, 2004.

541 Yang, Q., Li, X. Q., Zhou, X.Y., Zhao, K. L., Ji, M., and Sun, N.: Investigation of the
542 ultrastructural characteristics of foxtail and broomcorn millet during carbonization and its
543 application in archaeobotany, *Chinese. Sci. Bull*, 56(14), 1495-1502, 2011a.

544 Yang, Q., Li, X. Q., Liu, W. G., Zhou, X.Y., Zhao, K. L., and Sun, N.: Carbon isotope
545 fractionation during low temperature carbonization of foxtail and common millets, *Org.*
546 *Geochem.*, 42, 713-719, 2011b.

547 Yang, L. H., Wang, T., Zhou, J., Lai, Z. P., and Long, H.: OSL chronology and possible forcing
548 mechanisms of dune evolution in the Horqin dunefield in northern China since the Last Glacial
549 Maximum, *Quatern. Res.*, 78, 185-196, 2012.

550 Yang, Q., and Li, X. Q.: Investigation of the controlled factors influencing carbon isotope
551 composition of foxtail and common millet on the Chinese Loess Plateau, *Sci. China Ser D*,
552 58(12), 2296-2308, 2015.

553 Yang, Q., Li, X.Q., and Zhou, X.Y.: Vegetation Succession Responding to Climate Changes since
554 LGM in Desert-Loess Transition Zone, North China, *Acta. Antherop. Sin.*, DOI:
555 10.16359/j.cnki.cn11-1963/q.2015.0000, in Chinese with English abstract , 2015.

556 Zhang, R and Liu, X. D.: An analogy analysis of summer precipitation change patterns between
557 mid-Holocene and future climatic warming scenarios over East Asia, *Sci. Geogr. Sin.*, 29(5),
558 679-683, in Chinese with English abstract, 2009.

559 Zhao, J. B.: Soil developed in the Holocene Megathermal and climatic migration in the
560 Guanzhong area, *Sci. Geogr. Sinia*, 23(5), 554-559, 2003. (in Chinese with English abstract).

561 Zhao, Z. J., and Xu L. G.: The tentative flotation result and preliminary analysis in Zhouyuan
562 ruins (Wangjiazui site), *Cult. Rel.*, (10), in Chinese, 89-96, 2004.

563

564 **Tables**565 **Table 1 Sampling sites and the number of common millet samples**

Sites	Location	Cultural types	Sample source	<i>n</i>
Baijia	34°33'7.53"N 109°24'38.6"E	Early Laoguantai Culture	Cultural layer	12
Huiduipo	34°34'4.1"N 109°01'41.8"E	Banpo type, Yangshao Culture	Cultural layer	9
Manan	34°28'23.7"N 109°05'17.5"E	Miaodigou type, Yangshao Culture	Cultural layer	11
Beiniu	109°19'2.6"E	Longshan Culture	Cultural layer	15
Nansha	34°29'30.1"N 109°42'47.9"E	Erlitou Culture, Shang Dynasty	Cultural layer	20

566 *n* means the number of remnant common millet samples derived from the section.

567

568

569 **Table 2 Accelerator mass spectrometry (AMS) dates from Baijia (BJ), Huiduipo (HDP),**570 **Manan (MN), Beiniu (BN), and Nansha (NS)**

Sample code	Depth (cm)	Sample type	Radiocarbon age (¹⁴ C yr BP)	Calibrated age range (cal yr BP, 2σ)	Lab code
BJ-15	180-190	Common millet	6,705±40	7,504-7,657	OZM447
BJ-2	50-60	Charcoal	6,675±40	7,476-7,612	OZM446
HDP-13	235-250	Common millet	5,720±50	6,408-6,639	OZM473
HDP-9	160-180	Rice seed	5,015±45	5,655-5,896	OZM472
HDP-5	80-100	Rice seed	5,120±35	5,750-5,831	OZM471
HDP-3	40-60	Foxtail millet	5,185±40	5,891-6,009	OZM470
MN-8	140-160	Foxtail millet	4,550±35	5,053-5,191	OZM452
BN-13	280-300	Foxtail millet	5,450±70	6,172-6,400	OZM481
BN-10	220-240	Foxtail millet	3,820±45	4,138-4,360	OZM480
BN-8	180-200	Rice seed	3,770±35	4,073-4,244	OZM479
BN-5	120-140	Foxtail millet	4,540±50	5,040-5,323	OZM478
BN-1	40-60	Common millet	4,110±40	4,521-4,730	OZM477
NS-15	230-240	Wheat seed	3,300±30	3,454-3,593	OZM460
NS-11	200-210	Wheat seed	3,280±35	3,445-3,587	OZM459
NS-5	140-150	Wheat seed	3,300±30	3,454-3,593	OZM458

571 All assays were run on the STAR Accelerator, ANSTO, Australia. Calibrations refer to the

572 Radiocarbon Calibration Program (Reimer et al., 2013).

573

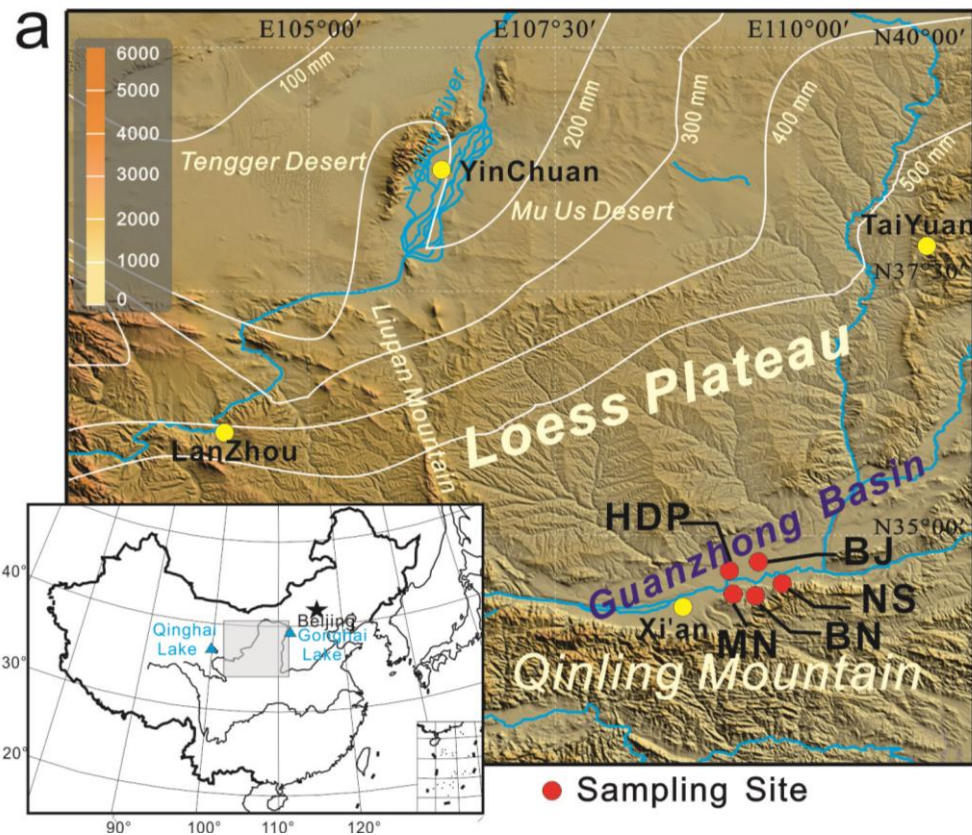
574 **Table 3 Information for grouped common millet remains, by section**

Section	Cultural age	Depth (cm)	<i>n</i>	Calibrated ages (cal yr BP)	Mean δ ¹³ C(‰)	Corrected δ ¹³ C (‰)	P _{gs} (mm)
Baijia	Laoguantai Culture	50-190	12	7,476-7,657	-10.4±0.2	-12.2±0.2	336±30
Huiduipo	Banpo type, Yangshao Culture	200-250	3	6,408-6,639	-10.6±0.3	-12.4±0.3	311±37
	Banpo type, Yangshao Culture	120-200	2	5,655-5,896	-9.6±0.1	-11.4±0.1	442±9

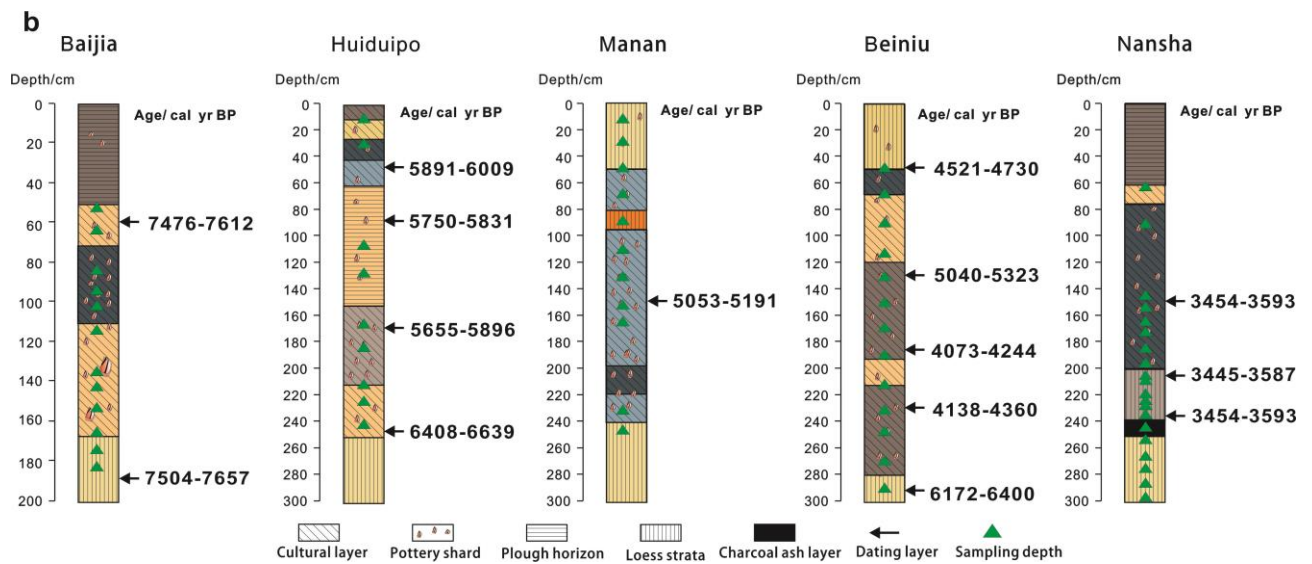
	Banpo type, Yangshao Culture	0-120	5	5,750-6,009	-9.9±0.1	-11.7 ±0.1	402±12
Manan	Miaodigou type, Yangshao Culture	0-260	11	5,053-5,191	-10.3±0.4	-12.1±0.4	346±47
Beiniu	Yangshao Culture	260-300	3	6,172-6400	-10.3±0.1	-12.1±0.1	349±8
	Longshan Culture	180-240	3	4,073-4,360	-9.9±0.1	-11.7±0.1	397±13
	Longshan Culture	80-180	4	5,040-5,323	-10.3±0.2	-12.1 ±0.2	352±27
	Longshan Culture	40-80	4	4,521-4,730	-10.6±0.2	-12.4±0.2	313±22
Nansha	Erlitou Culture, Shang Dynasty	50-300	20	3,445-3,593	-10.2±0.4	-12.0 ±0.4	346±47

575 *n* means the number of samples for $\delta^{13}\text{C}$ analysis. Corrected $\delta^{13}\text{C}$ means $\delta^{13}\text{C}$ value of millet being
576 corrected the $\delta^{13}\text{C}$ difference of atmospheric CO_2 between modern and Holocene for precipitation
577 reconstruction. P_{gs} means reconstructed precipitation of millet growth seasons.

578 **Figures**



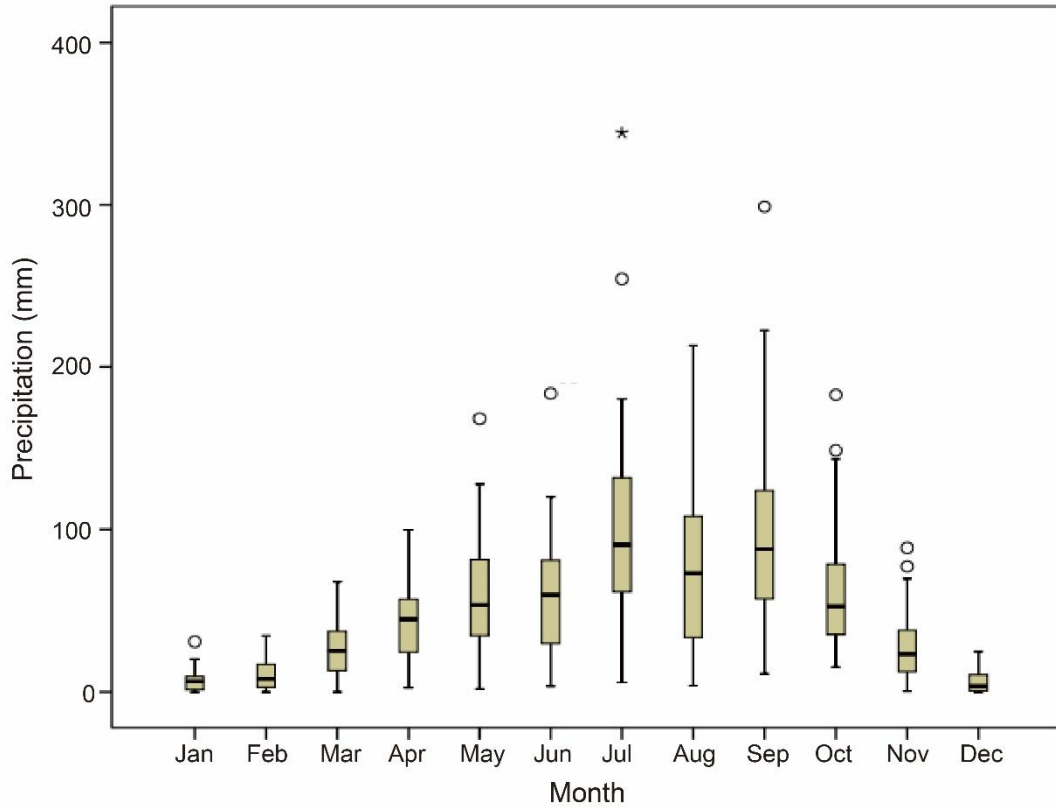
579



580

581 **Figure 1.** Location of sampling sites (Panel a) and description of all sampling sections (Panel b).
 582 Red solid circles indicate sampling sites: Baijia(BJ), Huiduipo (HDP), Manan (MN), Beiniu (BN),
 583 Nansha (NS).

584



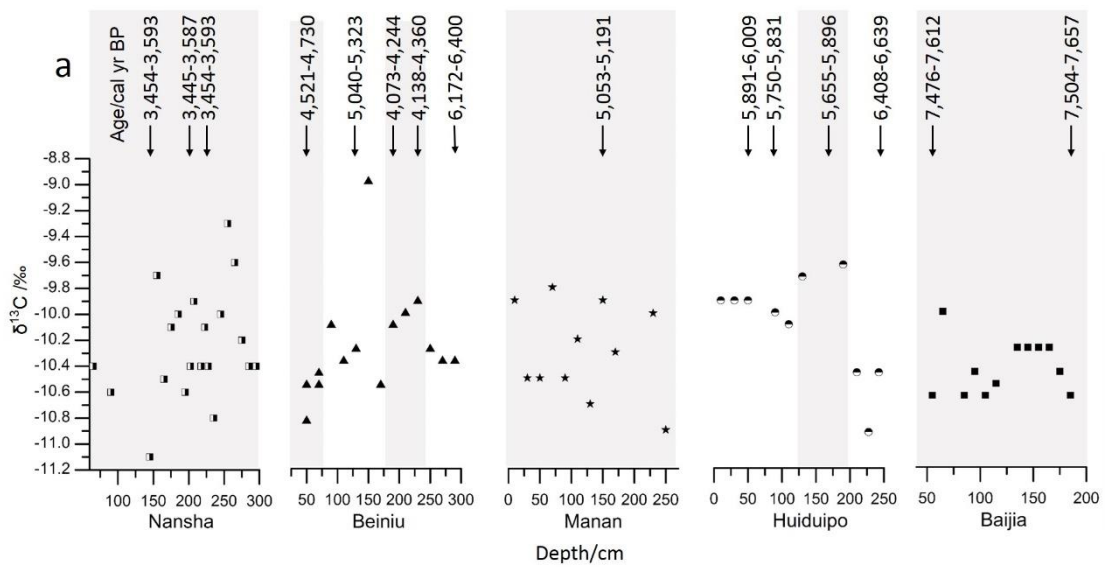
585

586 **Figure 2.** Instrumental precipitation data for 1951-2011 from Xi'an Station, Shaanxi, China
 587 (original data, Data Sharing Platform, China Meteorological Administration). The empty circle (o)

588 indicates an abnormal value; the asterisk (*) indicates an extremely abnormal value.

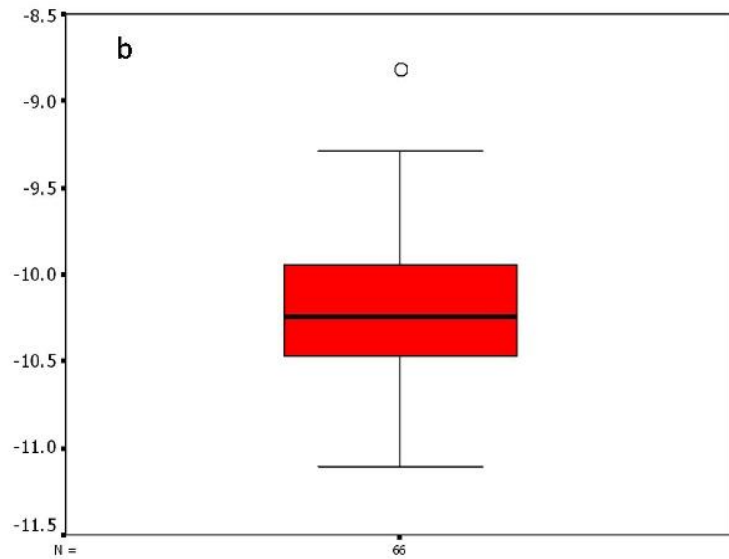
589

590



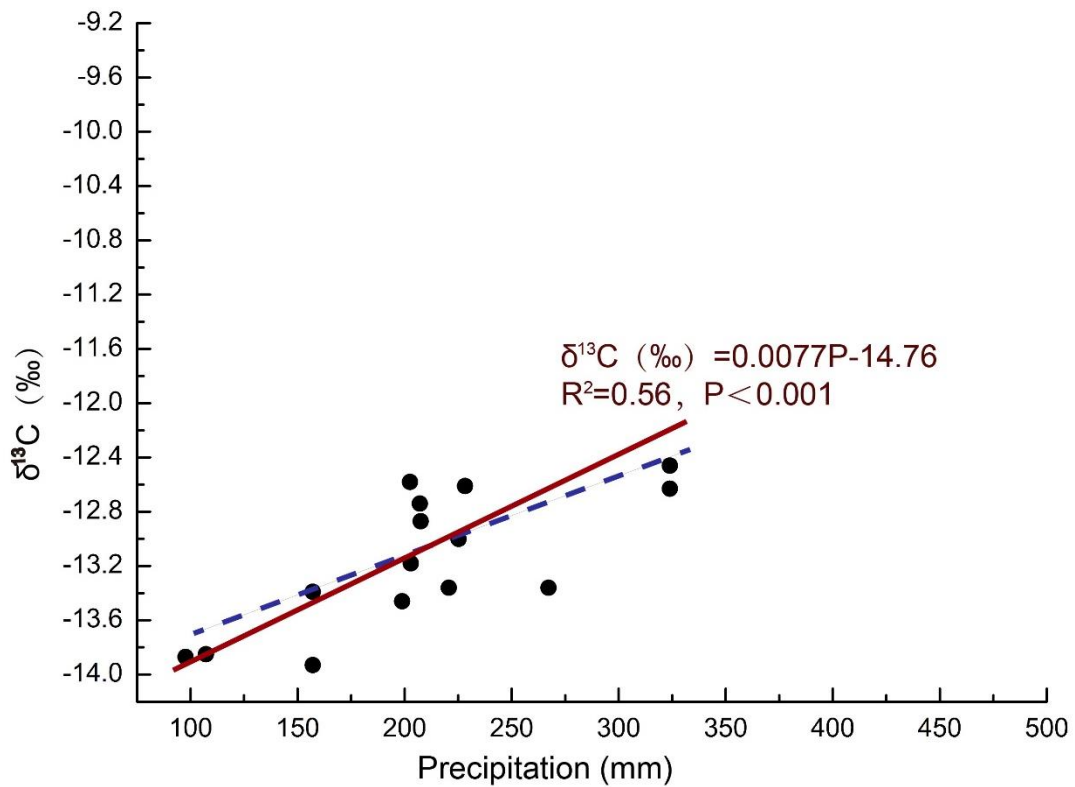
591

592



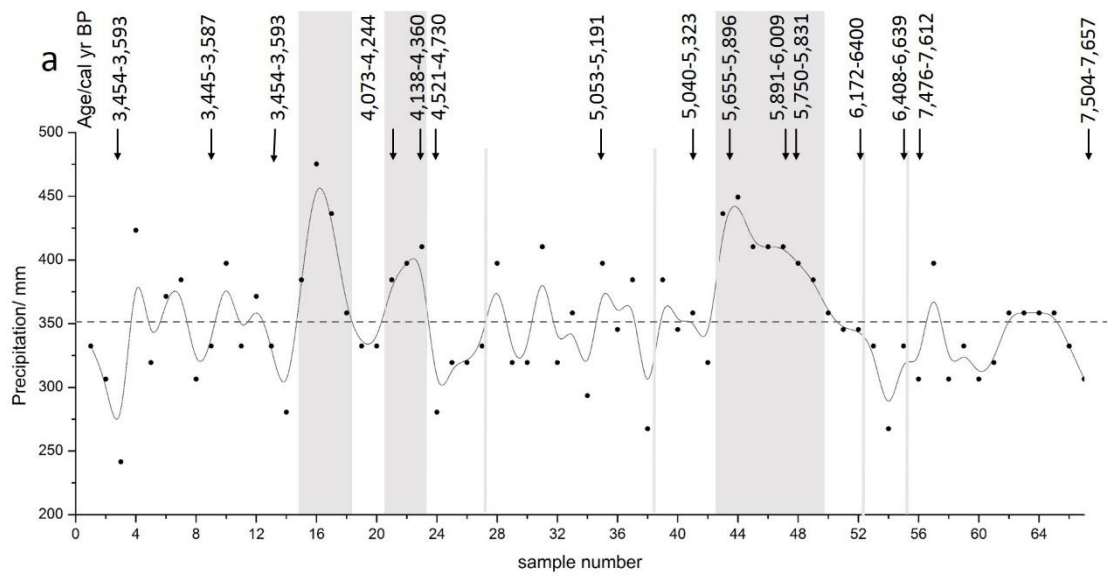
593
594
595
596
597
598

Figure 3. $\delta^{13}\text{C}$ of common millet from archeological sites, Guanzhong Basin. Panel a shows raw data points including all $\delta^{13}\text{C}$ and calibrated age range versus depth. The group division were expressed in gray or white color. Panel b shows Boxplot of all $\delta^{13}\text{C}$ of common millet, with the mean value $10.2 \pm 0.4\text{‰}$ ($n=66$, $\text{SD}=\pm 1 \sigma$) and the anomaly value of -8.8‰ excluded.

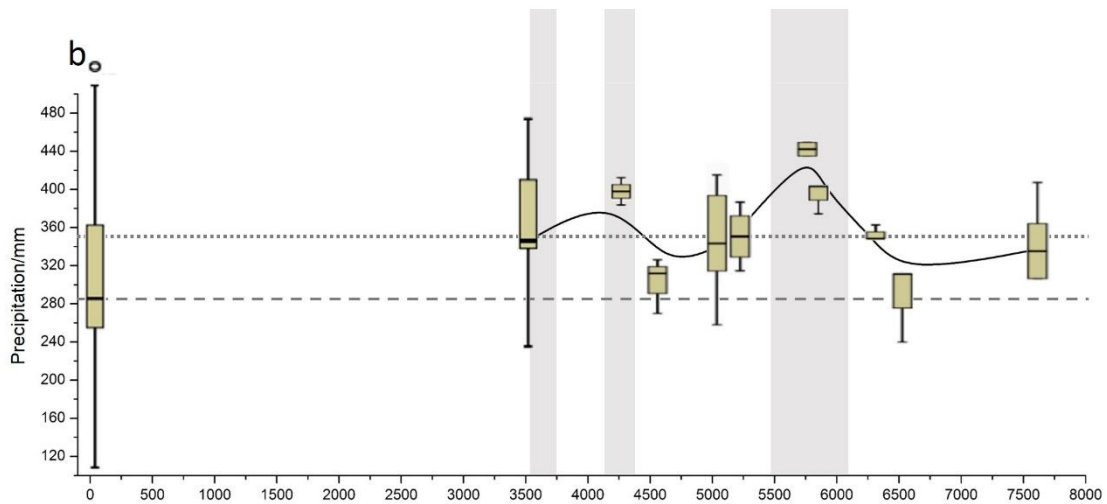


599
600
601
602
603
604

Figure 4. The regression model of the $\delta^{13}\text{C}$ of modern common millet and summer precipitation, which data from Yang and Li (2015). Dark red line denotes the line of best fit established using SMA; the blue dotted line denotes the line of best fit established using OLS.



605



606

607

608

609

610

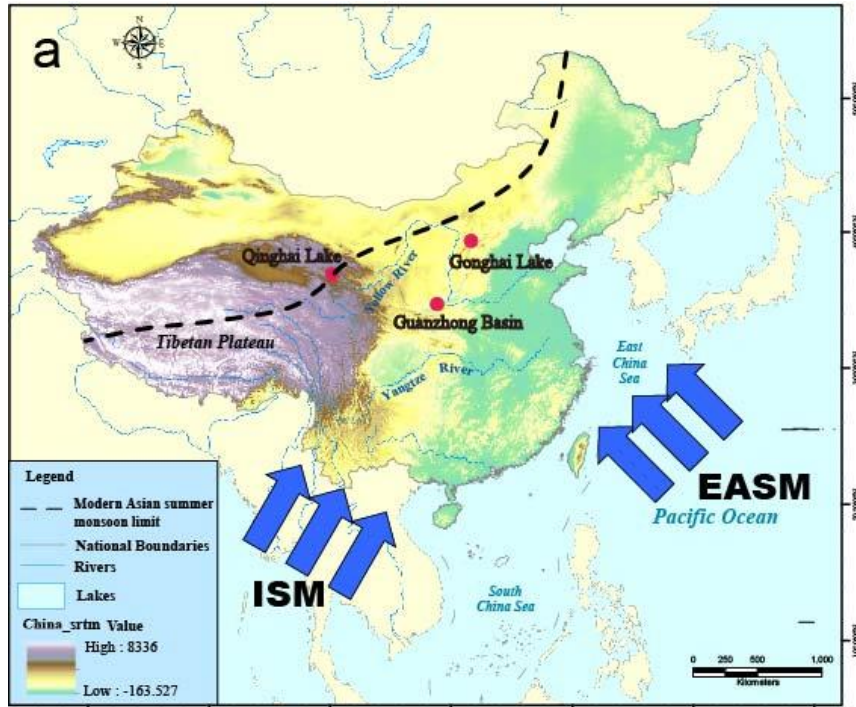
611

612

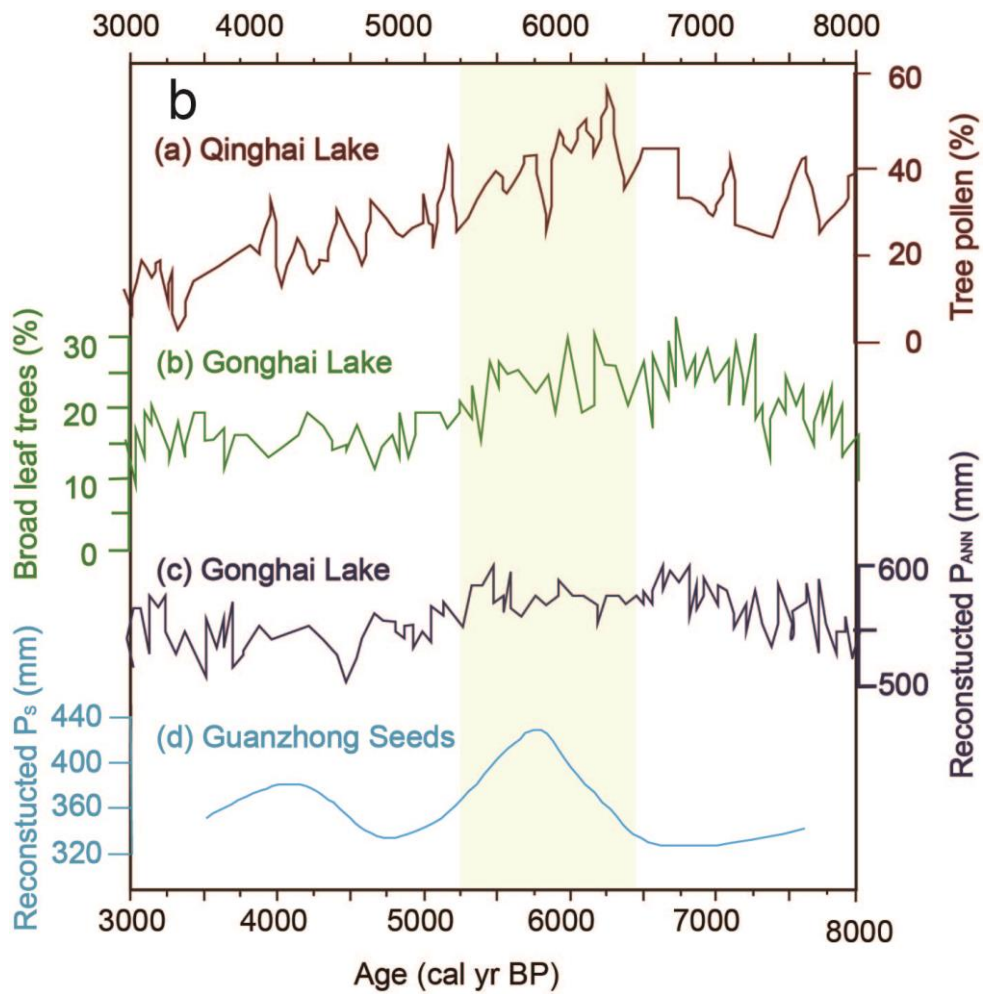
613

614

Figure 5. Reconstructed summer precipitation during 7.7-3.4 ka BP, Guanzhong Basin (Panel a) and comparison the reconstructed precipitation during the Holocene to precipitation for mid-June to September for a modern period in Xi'an city (original data for 1951–2011, from the China Meteorological Administration). The gray color in both panel a and b indicates the markedly humid periods during the Holocene. The gray line in panel a means the group division. The dot line in panel b indicates the mean precipitation of millet growth season at 7.7-3.4 ka BP; the dash line in panel b indicates the mean precipitation for mid-June to September during 1951-2011.



615



616

617 **Figure 6.** The modern Asian summer monsoon limit is shown by a dashed line in the map (panel

618 a). The red dots signed in the map are the locations of Qinghai Lake, Gonghai Lake and

619 Guanzhong Basin, whose precipitation were carried out comparison. Comparison of reconstructed
620 summer precipitation for 7.7-3.4 ka BP, Guanzhong Basin, with the pollen records of lakes
621 sediments from around the CLP. **(a)** Tree pollen percentages from Qinghai Lake (Shen *et al.*,
622 2005). **(b)** Broadleaf tree pollen percentages from Gonghai Lake (Chen *et al.*, 2015). **(c)**
623 Reconstructed annual precipitation from the pollen records of Gonghai Lake (Chen *et al.*, 2015).
624 **(d)** Reconstructed summer precipitation from the $\delta^{13}\text{C}$ values of common millet, Guanzhong
625 Basin.
626